Boron-SiC diffusion couple : thermodynamics and reactivity at high temperature

Y. Benamra, B. Gardiola, F. Robaut, O. Dezellus, F. Cauwet, L. Auvray, G. Ferro, J. Andrieux

Boron-SiC diffusion couple: thermodynamics and reactivity at high temperature

Y. Benamra [1], B. Gardiola [1], F. Robaut [2], O. Dezellus [1], F. Cauwet [1], L. Auvray [1], G. Ferro [1], J. Andrieux [1,*].

[1] Universite Claude Bernard Lyon 1, CNRS, LMI UMR 5615, Villeurbanne, F-69100, France

[2] Universite Grenoble Alpes, Grenoble-INP, CNRS, SIMaP, 38000, Grenoble, France

* corresponding author: jerome.andrieux@univ-lyon1.fr

Postal address: LMI-UMR 5615 CNRS / UCBL, Domaine Scientifique de la Doua ,Université Claude Bernard Lyon 1, Bâtiment Chevreul, 6 rue Victor Grignard, 69622 Villeurbanne CEDEX

Abstract

This study investigates the reaction between silicon carbide (SiC) and boron (B) at high temperature. A B/SiC diffusion couple treated at 1973 K (1700 °C) for 8 hours under uniaxial pressure was analyzed using energy dispersive spectroscopy and electron probe microanalysis with wavelength dispersive spectroscopy. Distinct reaction zones were identified, and the reaction sequence was established as SiC/(B_xC)/SiB_6/(SiB_n)/(β-B). This sequence aligns with B-C-Si phase equilibria and driving force calculations, which predict (B_xC) as the first phase formed between B and SiC. The formation of ternary solid solutions is also discussed, comparing reported Si solubility in (B_xC) and B solubility in SiC with our findings. The boron carbide layer exhibits a composition gradient (13.7 at.% C to 12.4 at.% C) and was identified as a ternary solution with an average silicon content of 2.0 at.%. This study is based on an unprecedented approach to interface reactivity in the B-C-Si system, relying on the experimental study of the B-SiC diffusion couple and thermodynamic calculations of phase equilibria. The results also highlight the relevance of the existing thermodynamic database for

predicting phase equilibria in this system. However, the composition range of (B_xC) and (SiB_n) may require further investigation.

1 Introduction

The B-C-Si ternary system and its associated phase equilibria have played a crucial role in the advancement of lightweight refractory ceramics and hard materials [1]: first, in understanding the sintering mechanisms of SiC with boron or carbon as sintering agents, and second, in utilizing silicon as a sintering agent for boron carbide [2]. The recent interest in boron carbide stems from its promising electronic properties, particularly its wide bandgap (1.6-2.2 eV [3]) in combination with its high neutron capture cross-section [4]. This makes it a potential candidate for heterostructures in nuclear and electronic applications. However, elucidating its exact electronic properties (essential data is still missing) [5–8] requires obtaining a monocrystalline boron carbide material, in either bulk or layer form.

In the latter case, carbide substrates are ideal for achieving (B_xC) heteroepitaxial growth thanks to their chemical compatibility. Some of the present authors recently reported the successful heteroepitaxial growth of boron carbide on 4H-SiC using chemical vapor deposition (CVD) at 1873 K (1600 °C) with BCl_3, C_3H_8, and H_2 gas mixtures [9, 10]. This was made possible by inserting a boronising step at a lower temperature (1473 K-1200 °C) before the epitaxial growth step, which implied surface conversion of the SiC substrate under a flux of BCl_3. Despite such success, the boronising reaction was found to be complex, with the formation of an amorphous boron-containing layer on top of the monocrystalline B_xC layer. This amorphous boron reacts and participates in the transient formation of other phases when the temperature rises but this did not affect the final CVD growth. As a consequence, the goal of the present work was to explore the thermodynamics and diffusion in the B-C-Si ternary system for a better understanding of the reactivity between boron and SiC. It is to note that the

boron sample used in the present work was polycrystalline rhombohedral boron. This work is a first step in understanding reactivity between boron and SiC, e.g. polycrystalline boron and SiC. This study is part of the framework of CVD experiments where amorphous boron was deposited on SiC substrates. But the aim of the present work is not a direct comparison with the CVD results. An interesting question, but out of the scope of the present paper, will be to study the reactivity of amorphous boron in contact with SiC and to compare it with the results of the present paper, together with the results of the CVD experiments [9, 10].

Experimental results of B-C-Si phase equilibria, obtained on precise composition equilibrated alloy samples, were first reported by Kieffer *et al*. [11] and thermodynamic modellings were later proposed by several authors [1, 12–15]. No stable ternary intermediate compound exists in the B-C-Si system according to the available literature [1, 15, 11]. Kieffer *et al*. [11] pointed out that the (B_xC) phase is the most stable with the existence of tie-lines with SiC and SiB_6 at 1973 K (1700 °C) (**Fig. 1a**) and 2173 K (1900 °C, not shown). They also reported the existence of a Si solubility in (B_xC) in three-phase equilibrium with SiC and boron silicide of about 4.3 at.% (8 h at 2073 K-1800 °C or 6 h at 2273 K-2000 °C) which is however not considered in most of the thermodynamic modelling of the system [1, 12–15]. In 2009, the modelling of the B-Si-C system was proposed by Chen *et al*. [16], based on their own description of the B-Si binary system and previous descriptions of the two other binary systems (B-C by Kasper [14] and Si-C by Gröbner *et al*. [17]). The thermodynamic calculations show discrepancies compared to the experimental observations by Kieffer *et al*. [11]. The thermodynamic database by Chen *et al*., for instance, led to the 1973 K (1700 °C) calculated isothermal section, as shown in **Fig. 1b**, which is compared to the experimental isothermal section by Kieffer *et al*. (**Fig. 1a**). The main difference is the nature of the equilibria regarding the (B_xC) phase. Whereas Kieffer *et al*. only described solid phase equilibria with (B_xC) (**Fig. 1a**), the thermodynamic modelling by Chen *et al*. indicated a liquid phase ($26 \leq$ at.% $B \leq 42$)

in equilibrium with (B_xC) (**Fig. 1b**). The second difference concerns the extension of Si solubility in (B_xC) which was not found to be as high as that reported by Kieffer *et al.*[11].

Zhao recently reviewed the diffusion couple technique and its value for investigating phase equilibria [18]. For one equilibrated sample, and for one temperature, this opens up the possibility for probing multiple compositions of alloys. It maps out a constitutional phase diagram with determination of the phase field boundaries as well as the direction of the tie-lines on the isotherm, ultimately establishing phase equilibria and relationships in multicomponent systems [19, 20]. To the authors' knowledge, despite its value, the diffusion couple technique has never been used to study phase equilibria and reactivity between boron and silicon carbide. To this end, a B-SiC diffusion couple was heat-treated at 1973 K (1700 °C) for 8 h. Such a sample allowed us to determine the solubility limits of B in SiC and Si in (B_xC) and (SiB_n) respectively. We also assessed the reliability of the thermodynamic database proposed by Chen *et al*. [16], particularly in the context of the CVD growth of (B_xC) on 4H-SiC.

2 Experimental work

Boron slices approximately 2 mm thick were used for the assemblies. These slices were obtained by cutting a large piece of pure polycrystalline rhombohedral boron provided by Koch-Light Laboratories (purity > 99.8 %) and were mirror-polished on both faces. The SiC used in these experiments consisted of high-purity monocrystalline 4H-SiC wafer pieces of 350 µm thickness from SiCrystal (https://sicrystal.de/index.php/en/). Before assembly, the native oxide was removed with HF cleaning. Sacrificial SiC substrates (SiC_{sac}), positioned above and below the SiC/B/SiC assembly, were used as diffusion barriers, as well as pyrolytic graphite (PyG) layers to prevent direct contamination of the B-SiC diffusion couple from the graphite molds

(30 mm diameter), the latter containing the whole assembly ($PyG/SiC_{sac}/SiC/B/SiC/SiC_{sac}/PyG$).

The B-SiC diffusion couple was obtained following an 8-hour (t = 8 h) heat treatment in a 1 bar regulated argon atmosphere at 1973 K (1700 °C) under a compressive stress of 17 MPa using a uniaxial hot press (HP) from Goliath Stein Heurtey Physitherm. During this high temperature step, and regarding the carbon rich atmosphere of the assembly, reaction between carbon monoxyde (from residual Oxygen) and the sample is also highly possible. In order to avoid surface contamination or inhomogeneity, a cross-sectional cut was made in the center of the diffusion couple, far from its edges.

The cross-sectional cut of the heat-treated diffusion couple was resin-mounted, mirror-polished, and characterized using scanning electron microscopy with energy dispersive spectroscopy (SEM-EDS) (FEI Quanta 250 FEG) and electron probe microanalysis with wavelength dispersive spectroscopy (EPMA-WDS) (Cameca SX100) to analyze the reactive interfaces and determine the phase compositions.

As EDS parameters, a beam energy of 5 kV with a 10 mm working distance and a 30 s time acquisition (point mode) were used. For these conditions, Monte-Carlo simulation of electron trajectory in solid boron was performed using CASINO v2.48 [21]. This defines a maximum volume for the electron's interactions with pure boron of 480x480x300 nm^3 for a collected X-ray intensity from a depth of around 150 nm. In addition, SiC, electronic grade, was used as a physical reference standard to quantify silicon content within the different phases whereas a C-rich B_xC, 20 at.% C, was used to determine boron and carbon contents. The quantitative procedure to determine the composition of the different phases used the PAP $\Phi(\rho z)$ model [22].

WDS measurements were conducted using a CAMECA SX100 electron microprobe equipped with four distinct vertical spectrometers. These included a TAP monochromator (2d = 25.75 Å) for quantification of Si, Al and Mg; a PC3 multilayer monochromator (Mo/B_4C, 2d = 200.5 Å) for B; a LiF monochromator (2d = 4.027 Å) for Mn and Fe; and a PC2 multilayer monochromator (Ni/C, 2d = 95 Å) for C. The measurements were performed at an accelerating voltage of 15 kV, with a counting time of 30 s (point mode), and a beam current of 50 nA. For these conditions, simulations based on electron interactions with pure boron define a maximum volume of 2500x2500x1800 nm^3 for a collected X-ray intensity from a depth of around 1400 nm [21]. All elementary quantifications were based on the intensities of the K_α spectral lines. The measurements were calibrated using pure Fe, Al, and Mn standards, as well as TiB_2 (for boron), SiC (for Si and C), and MgO (for Mg) standards. The quantitative procedure for analysing the samples used the PAP $\Phi(\rho z)$ model [22]. It is worth noting that Fe, Mg, Al, and Mn were detected as impurities, likely originating from the boron source, primarily identified in the boron-rich phases (β-B) and (SiB_n), and measured compositions were below 0.23 at.%Fe, 0.13 at.%Mg, 0.07 at.%Al, and 0.03 at.%Mn, respectively.

Isothermal sections, chemical potential diagrams, and driving force calculations were performed using the *Thermo-Calc* software v2022b [23] and the B-C-Si thermodynamic database developed by Chen *et al*. [16].

3 Literature review of the systems

The most recent thermodynamic modelling of the B-C-Si ternary system comes from the work by Chen *et al*. [16] and an example of an isothermal section calculated at 1973 K (1700 °C) is given in **Fig. 1b**. This considers the solubility of the third element in each of the binary phases and it will be used in this work as a framework for understanding the reactivity between B and SiC phases and supporting discussion of phase equilibria at atmospheric pressure. Chen *et al*.

based their thermodynamic modelling on the thermodynamic descriptions of C-Si by Gröbner *et al*. [17] and B-C by Kasper [14], as well as on a reassessment of the B-Si binary system at atmospheric pressure, as described in the following sections.

3.1 C-Si system

Within the C-Si system, the only intermediate phase identified is silicon carbide (SiC). SiC exists in various forms called polytypes, which are broadly categorized as β-SiC and α-SiC [24]. β-SiC, also called 3C-SiC, crystallizes in a cubic $F\bar{4}3m$ space group (a=435 pm [15]), while the α-SiC designation includes both hexagonal $P6_3mc$ (4*H-type SiC*; a=307 pm; c=1005 pm [25] and 6*H-type SiC*; a=308 pm; c=1510 pm [15]) and rhombohedral $R\bar{3}m$ (*R-type SiC*; a=308 pm; c=605 pm [15]). For the thermodynamic description, a single analytical Gibbs-energy description was used for both α- and β-SiC, based on a two-sublattices model as $(Si)_1(C)_1$ [17]. The line compound was stable up to 3096 K (2823 °C) where it decomposed into liquid and graphite by incongruent melting. C solubility in the liquid phase was rather limited up to 2273 K (2000 °C) [26].

3.2 B-Si system

In the B-Si binary system, two intermediate line compounds have been reported, namely SiB_3 and SiB_6 (SiB_3: $R\bar{3}m$, a=631.9 pm, c=1271.3 pm; SiB_6: *Pnnm*, a=1439.7 pm, b=1831.8 pm, c=991.1 pm [15]). SiB_3 is expected to transform into Si (Diamond_A4) and SiB_6 by peritectoid transformation at 1543 K (1270 °C) whereas SiB_6 is stable up to 2123 K (1850 °C).

On the boron-rich side, the precise nature of the boron-silicon phases has been a topic of debate in the literature, including two major studies in the 1980s. Viala *et al*. [27] reported the existence of a rhombohedral β-boron silicon-enriched solid solution, denoted (β-B) hereafter, with solubility of silicon up to 5.6 at.% , found from their X-ray diffraction (XRD) and EPMA analyses of reaction-sintered samples prepared at 1873 K (1600 °C). They observed a regular increase in the cell parameter *a* from 1092.6 pm for pure rhombohedral β-boron to 1111 pm for (β-B) with 5.6 at.% Si at 1873 K (1600 °C). Their observations emphasize that the *c* parameter variation falls within the measurement uncertainty (0.25 %). Their work also suggests that the silicon solubility in (β-B) reaches up to 6.13 at.% Si at 2137 K (1864 °C) and that the silicon-saturated β-boron solid solution is in equilibrium with SiB_6.

On the other hand, several authors [15,28,29,30,31] have proposed the existence of an intermediate B-Si solid solution based on the work by Armas *et al*. [32] and Male and Salanoubat [33]. The latter authors conducted high-temperature liquidus measurements using Simple Thermal Analysis on B-rich B-Si samples and attributed a break in the liquidus curve at 2293 K ± 15 K (2020 °C) to the incongruent melting of a boron-silicon phase, named hereafter (SiB_n). At this temperature, the (SiB_n) phase (around 4 at.% Si) decomposed into a liquid phase (9.3 ± 0.4 at.% Si) and a (β-B) solid solution containing 3 ± 0.4 at.% Si. Armas *et al*. thus suggested a distinction between the (SiB_n) and (β-B) phases, respectively. They also conducted XRD and EPMA analyses on equilibrated samples prepared at 1873 K (1600 °C), 2173 K (1900 °C), and 2273 K (2000 °C). The (SiB_n) solid solution ($R\bar{3}m$, a=1100 pm, c=2385 pm for 3.2 at.% Si [32]) exhibited an isotypic relationship with the silicon-enriched solid solution (β-B) ($R\bar{3}m$). Its composition range has been estimated to be between 1.6-5.4 at.% Si at 1873 K (1600 °C) [32]; 2-6.25 at.% Si at 1973 K (1700 °C) [34]; 3-5.7 at.% Si at 2173 K (1900 °C) and 3.3-4.5 at.% Si at 2273 K (2000 °C) [32], and the maximum solubility value has been determined as 6.25 at.% Si at 2123 K (1850 °C) [32].

Questions arise regarding the temperature uncertainty in liquidus measurements, together with the choice of the inflection point which is not discussed in the article by Armas *et al*. [32]. Different conclusions were also obtained compared to the XRD studies by Viala *et al*. [27]. This suggests that a new and thorough study may be needed to bring new information on this point. However, to ensure consistency with the established literature since the 1980s and in the absence of evidence contradicting the existence of (SiB_n), the latter phase was considered and was distinguished from (β-B) in this work. As a consequence, this suggests that the SiB_6 phase is in equilibrium with the (SiB_n) phase and that the existence of (SiB_n) significantly reduces the composition range for (β-B) proposed by Viala *et al*. [27]. Armas *et al*. [32] suggest that the (β-B)+(SiB_n) two-phase field is probably very narrow and was not clearly observed. The following composition/temperature sets belong to the (β-B) single phase domain: 0.8 at.% Si at 1873 K (1600 °C) [32]; 1 at.% Si at 1973 K (1700 °C) [34]; and 2.4 at.% Si at 2273 K (2000 °C) [32]. The thermodynamic model used by Chen *et al.* [16] to describe the Gibbs energy of the (SiB_n) phase is a three sub-lattice model as $(B)_{61}(Si)_1(B,Si)_8$. In addition, the (β-B) phase is described in the B-Si binary system by a two sub-lattice model where Si substitutes boron on the second sub-lattice: $(B)_{93}(B,Si,Va)_{12}$ [16].

3.3 B-C system

The boron-carbide phase was described in the B-C binary system as an intermediate solid solution with a composition range of $B_{12+x}C_{3-x}$ ($0.06 < x < 1.7$) [35]. It will be labeled (B_xC) in this work whereas B_4C or $B_{13}C_2$ define a given composition. It melts congruently at 18.4 at.% C and 2725 K (2452 °C). It crystallizes in the trigonal system, space group $R\bar{3}m$, with cell parameters varying within the range $560.7 < a < 565.1$ pm and $1209.5 < c < 1219.6$ pm for a C composition range from 9 to 20 at.% C [15]. The simplified structure of (B_xC) consists of B_{12}

icosahedral units and C-B-C or C-B-B linear chains. While increasing the C content, there is a partial substitution in the icosahedral units resulting in the formation of $B_{11}C$ units and a decrease in the boron content within the chain [3, 6, 36]. The thermodynamic model described by Kasper [14] and adopted in Chen *et al.* modelling for (B_xC) is a two sub-lattice model such as $(B_{12},B_{11}C)_1(B_2Va,C_2B,B_2C)_1$ considering the crystal structure of (B_xC) [14, 37] and the results of Werheit *et al*. [38]. In addition, Rogl *et al.* [37] reported C solubility in an (β-B) rhombohedral phase up to 1.43 at.% C where the latter decomposed by incongruent melting at 2373.6 K (2100.6 °C). This is considered in the modelling proposed by Kasper where the (β-B) phase is described in the B-C binary system by a two sub-lattice model where C substitutes boron on the second sub-lattice: $(B)_{93}(B,C,Va)_{12}$ [14, 37].

3.4 Solubilities of a third element in binary phases

It has already been mentioned that no ternary phase is reported in the literature. Therefore, the description of the ternary system is based on the binaries and the solubility of B in SiC, Si in (B_xC) and C in the (SiB_n) compounds.

3.4.1. Solubility of B in SiC

The solubility of boron in SiC shows dependence on the crystalline structure, as detailed in **Table 1**. Literature data suggests a wider range of solubility for β-SiC (up to 3 at.%) compared to α-SiC (typically below 0.7 at.%).

Gao *et al*. [44] reported that solubility may also depend on the substitutional sites. Electron spin resonance studies, carried out by Woodbury and Ludwig [45], indicate a substitutional mechanism where B substitutes C in SiC. On the other hand, More *et al*. [46] reviewed literature

results [41, 47, 42] and found that SiC lattice contraction when incorporating boron suggests that B substitutes Si, while Tajima and Kingery [48] reported that B substitutes both Si and C. The recent modelling of the B-C-Si system by Chen *et al*. describes the SiC phase using a two sub-lattice model where B substitutes C : $(Si)_1(B,C)_1$ [16]. According to their work, the solubility of boron in SiC can extend into the ternary phase diagram up to 1.4 at.% B at 1973 K (1700 °C).

While incorporating B into SiC can affect its electrical properties, the behaviour is complex. Boron acts as an acceptor, introducing p-type doping characteristics into SiC [49]. When substituted for silicon, it constitutes a shallow level in 4H-SiC, while it gives a deep level when it substitutes for carbon [44, 50]. Pai *et al*. [51] studied a B-doped 4H-SiC porous sample and reported an increase in electrical conductivity, and specified that the figure of merit of the p-type B-doped SiC sample was lower than that of the n-type SiC.

Much research has been focused in the literature on heavily boron-doped silicon carbide. When the concentration of boron introduced by doping exceeds the solubility limit of B in SiC (**Table 1**)**,** a two-phase equilibrium B_xC-SiC was always reported after high temperature annealing. Linnarsson *et al*. [43] observed the formation of B_xC within heavily boron-doped 4H-SiC epitaxial layers annealed at temperatures ranging from 1973 to 2273 K (1700 to 2000 °C). Oriented platelets, characterized as a B_xC phase with $B_{13}C_2$ stoichiometry, have been identified within boron supersaturated 3C-SiC epitaxial layers annealed at 1873 K (1600 °C) [52]. A similar study [40] revealed a B_xC phase reported as $B_{13}C_2$ in the context of 2-3 at.% boron doping of a 3C-SiC substrate at 673 K (400 °C), followed by one-hour annealing at 1673 K (1400 °C).

3.4.2. Solubility of C in (SiB_n)

Literature data about the solubility of C in (SiB_n) is rather scarce. Only Roger *et al*. [30] have determined a carbon content of 1.1 at.% in a phase with $R\bar{3}m$ space group that they identified as (SiB_n). They concluded there was a slight decrease in the cell parameter *c* of the (SiB_n) phase ($SiB_{30.4}C_{0.35}$; c = 2386.25 pm). However, this was not considered in the modelling by Chen *et al*. [16], which used a strictly binary description with the three sub-lattices model previously described for a (SiB_n) phase in the B-Si system.

3.4.3. Solubility of Si in (B_xC)

Telle [2] experimentally measured a maximum solubility of 2.5 ± 0.3 at.% Si in (B_xC) and determined the Si solubility in (B_xC) as a function of the different observed phase equilibria at 2323 K (2050 °C), whereas at least 4.3 at.% Si was obtained by Kieffer *et al*. at 2273 K (2000 °C) [11]. The solubility of Si in (B_xC), especially for temperatures below 2273 K (2000 °C), is still under debate because the literature data is rather limited. However, it is accepted that Si preferentially substitutes carbon in the linear C-B-C chains [2, 38, 53], a more favorable position than B-sites in the icosahedral structural unit [54]. As a result, the thermodynamic model proposed by Chen *et al.* for the (B_xC) phase containing Si is the following two sub-lattice model $(B_{12},B_{11}C)_1(B_2Va,C_2B,B_2C,Si_2)_1$. This model, introducing the Si_2 species, is consistent with the crystal structure of (B_xC) described by Werheit *et al*. [38]. From their thermodynamic modelling, Chen *et al*. calculated maximum Si solubility, about 1.1 at.% Si, obtained when (B_xC) (12.8 at.% C) was in equilibrium with the liquid phase at 1973 K (1700 °C) [16].

4 Results

A large part of the B/SiC diffusion couple is presented in **Fig. 2a**, while **Fig. 2b** is a magnification of the upper SiC/B reactive interface.

First, **Fig. 2** unequivocally validates the reactivity between B and SiC at 1973 K (1700 °C) for 8 hours at 17 MPa. The grey contrast observed on the backscattered electron (BSE) images distinctly emphasizes the chemical contrast between the layers. EDS identifies the two noticeably light grey layers at the top and the bottom as SiC (marked as SiC-top and SiC-bot, respectively, in **Fig. 2a**). The development of an almost symmetrical and thick reaction zone between the two SiC layers is discernible. This indicates the intimate atomic-scale contact between B and SiC during the high-temperature 8-hour treatment. Multiple cracks were observed in the diffusion couple, believed to have formed during the cooling step due to the thermal expansion mismatch between the starting materials [55, 56] and the inherent brittle behaviour of formed phases [27].

Because of the symmetry of the reaction zone, the composition measurements were then focused on the upper SiC/B interface (**Fig. 2b**). The reaction layers displayed homogeneity in terms of chemical contrast and microstructure and were thus considered single-phase layers. This was further confirmed by EDS and EPMA-WDS measurements (**Table 2**).

The diffusion couple was carefully scanned to conduct composition measurements within a region exhibiting fewer cracks. No oxygen contamination was detected in any of the layers. The quality of the measurements, especially the low standard deviation, confirms the suitability of the selected area for analysis. Scan lines were conducted parallel to the interfaces (as schematized by the dashed lines in **Fig. 2**) to obtain the composition of each layer at the interfaces, and the results are summarized in **Table 2**. Also, **Fig. 3** presents the overall EDS composition profiles from the upper SiC substrate ("*SiC-top*", **Fig. 2**), along a scan line perpendicular to the interfaces, to the center of the diffusion couple.

The SiC at the (B_xC) interface was found to be stoichiometric. Within the detection limit of EDS measurements, no noticeable boron content was detected. Interestingly, no cracks were observed along the SiC/(B_xC) interface. Few cracks were observed through the SiB_6 layer perpendicular to the (B_xC)/SiB_6 interface which might be due to the reported disparities in thermal expansion coefficients in the literature [55, 56].

The (B_xC) layer (layer 2, **Fig. 2**) has a thickness ranging from approximately 140 to 160 µm. At the SiC/(B_xC) interface, the carbon content in (B_xC) was measured at 13.7 ± 0.2 at.% C, while at the (B_xC)/SiB_6 interface, it was found to be 12.4 ± 0.2 at.% C. Based on both EPMA and EDS measurements, it was observed that the boron content in the boron carbide layer increased at the expense of carbon as shown in **Fig. 4**.

However, **Fig. 4** and **Table 2** point out a difference in composition between EDS and EPMA measurements. For example, EDS found 83.2 ± 0.4 at.% B whereas EPMA measurements found 84.5 ± 0.2 at.% B at the SiC/(B_xC) interface. This difference in composition is higher than the precision measurement, indicating an accuracy difference. The EDS and EPMA measurements were conducted under different experimental conditions. The calibration standards were of different nature as detailed in the experimental section. However, the main difference was in the acceleration voltage used, 5 kV for EDS *versus* 15 kV for EPMA, leading to an interaction volume 163 times higher in EPMA than in EDS. The improved statistics of electron/matter interactions for EPMA results in better accuracy for this measurement, although at the expense of the experiment's spatial resolution. In addition, the total amount of B, C and Si for EPMA measurements at both (B_xC)/SiC and (B_xC)/SiB_6 interfaces was 99.7 ± 0.2 wt.% whereas EDS total amount varied almost linearly and ended with 103.1 ± 0.6 wt.% at the (B_xC)/SiC interface and 100.9 ± 0.5 wt.% at the (B_xC)/SiB_6 interface (**Table 2**). Compositions were then normalized

to 100 at.% in both cases. Keeping this in mind, EDS experiments remain interesting for following the relative evolution of the composition profiles through the overall sequence of reaction layers (**Fig. 3**) and particularly through the (B_xC) layer (**Fig. 4**). However, the EDS total amounts being larger than 100 wt.% suggest that the absolute carbon content determined by EDS on the C-rich side of the (B_xC) layer might be overestimated. For those reasons, EPMA compositions were chosen for their accuracy and used in the following to define the composition of the different phases at thermodynamic equilibrium, unless otherwise stated.

Considering the minor fluctuation in silicon across the (B_xC) layer (about 0.4 at.% Si, **Table 2**), a series of line measurements was conducted via EPMA in a direction perpendicular to the (B_xC)/SiC interface (**Fig. 5**). These measurements reveal a silicon composition gradient with a Si content of 1.8 ± 0.1 at.% at the SiC/(B_xC) interface and a value of 2.2 ± 0.2 at.% at the (B_xC)/SiB_6 interface.

A thin layer of stoichiometric SiB_6 (30-50 µm) was observed in equilibrium with boron carbide (layer 3, **Fig. 2** and **Table 2**) at the boron-rich side. From there to the center of the diffusion couple no more carbon was detected within the phases.

When scanning along the "*4-top"* layer, a boron rich phase, considered as the silicon boride (SiB_n) phase, was observed in equilibrium with SiB_6, with a composition of 5.4 at.% Si and no carbon detected. Furthermore, the "*4-mid*" line corresponds to the middle of the diffusion couple, and EDS measurements showed a composition of 99.5 at.% B and 0.5 at.% Si (**Table 2**). This reveals a gradient of composition with the decrease of silicon content through the silicon boride layer. Consequently, a careful line scan (with a mean distance between the EPMA measurements of around 7µm) was performed from the SiB_6 inner interface toward the center of the diffusion couple on a typical length of 300 µm and the resulting Si composition profile is shown in **Fig. 6**.

5 Discussion

Analysis of the diffusion couple at 1973 K (1700 °C) between boron and SiC, after SEM observations (**Fig. 2**) and detailed EDS/EPMA composition measurements (**Table 2**), revealed a reaction layers sequence determined as SiC/(B_xC)/SiB_6/(SiB_n)/(β-B). Experimental EPMA phase compositions at interfaces are reported in the isothermal section of the B-C-Si system calculated at 1973 K (1700 °C) according to the modelling by Chen *et al*. [16], and an experimental reaction layer sequence is proposed as the blue dashed line (**Fig. 7b**). The extension of the (B_xC) solid solution in the ternary B-C-Si at 1973 K (1700 °C), based on the literature and the present work, is proposed as the grey colored area in **Fig. 7a** and **Fig. 7b**, respectively. Experimental composition measurements underline the main differences in composition compared to the literature. In the B-C-Si system, most of the phases are involved in two-phase equilibria with the most stable phase at 1973 K (1700 °C) which is the (B_xC) solid solution. The following discussion will therefore consider them one by one, starting from the side rich in C and going towards the other.

A primary concern is the composition of (B_xC) in equilibrium with SiC. Chen *et al*. predicted that the Si solubility in (B_xC) might be less than 10^{-5} at.% at 1973 K (1700 °C) and that the carbon content of (B_xC) might be 20 at.% C considering an equilibrium with stoichiometric SiC [16], whereas B-rich SiC (1.4 at.% B) might be in equilibrium with a (B_xC) phase containing 18 at.% C and 0.09 at.% Si (**Fig. 1a**). The Si content found in this work was about 200 times higher (1.8 at.% Si) for (B_xC) with a carbon content of 13.7 at.% C (**Table 2**) in equilibrium with SiC. This value even exceeds the maximum solubility limits of Si in (B_xC) at 1973 K (1700 °C) predicted using the thermodynamic modelling by Chen *et al*., which is about 1.1 at.% Si at this temperature. While no experimental result regarding the solubility of Si in (B_xC) at equilibrium has been precisely documented in the literature at 1973 K (1700 °C), the value

found in this work (1.8 at.% Si) aligns well with the reported value of 2.2 ± 0.3 at.% Si (82.25 at.% B; 15.54 at.% C) at 2323 K (2050 °C) for $B_{12}(B,C,Si)_3$ phase (B_xC-type) in ternary equilibrium with liquid and SiC by Telle [2]. In addition, Telle also measured the composition of the (B_xC) phase in ternary equilibrium at 2323 K (2050 °C) with SiC and C (0.067 at.% Si; 19.29 at.% C; 80.64 at.% B). Finally, Telle [2] established, as the present work, that stoichiometric SiC is in equilibrium with different (B_xC) compositions as shown on **Fig. 7b**. From a structural point of view, an increase in the Si content of (B_xC) from the C-rich side of the solid solution compared to the values obtained by Chen *et al*. [16] is correlated to a higher elongation of the c-axis and, thus, to an increase in the aspect ratio c_0/a_0 as measured by Telle [2]. The latter author concludes that Si substitutes for C in the linear C-B-C chain explaining this increase in the c_0/a_0 aspect ratio.

In this study, no boron was detected in SiC within the EDS measurement limits. This result agrees with the other experimental measurements in the literature for α-SiC (**Table 1**). One of the most detailed studies from Linnarsson *et al*. [43] proposed a value of $1.9x10^{19}$ at/cm^3 for the solubility of B in SiC, i.e. a value lower than 0.02 at.% B at 1973 K (1700 °C) and thus lower than the EDS detection limit.

The second important point is the discussion of the phase equilibria on the B-rich side of the (B_xC) solid solution. Within the 8 h-1973 K (1700 °C) diffusion couple, a (B_xC)/SiB_6 interface was observed and the (B_xC) composition at this interface was measured as 85.4 at.% B, 12.4 at.% C and 2.2 at.% Si (**Table 2**). To the authors' knowledge, no study reports composition value at 1973 K (1700 °C) for such two-phase equilibrium as well as for the (B_xC) in three-phase equilibrium with liquid and SiB_6. Telle [2] observed a (B_xC) phase with the following composition: 90.27 at.% B, 8.93 at.% C, and 0.8 at.% Si in three-phase equilibrium with liquid

and SiB_n ("SiB_{14}" phase) at 2323 K (2050 °C), given that the measurement temperature (2323 K) was above the incongruent melting of SiB_6 at 2123 K (1850 °C).

Schreinemaker's rule suggests, as shown in **Fig. 7b**, that the composition of the (B_xC) phase at 1973 K (1700 °C), in the ternary equilibrium with liquid and SiB_6 (open circle, **Fig. 7b**) might be richer in silicon than the composition of (B_xC) in the (B_xC)-SiB_6 two-phase domain (blue diamond, **Fig. 7b**). Interestingly, it is suggested that the composition of the (B_xC) phase in the LIQ-(B_xC)-SiB_6 ternary equilibrium might reach at least the same value of Si content as that of the (B_xC) phase in the (B_xC)-SiC-LIQ ternary equilibrium. Up to now, the exact composition of the (B_xC) phase in the ternary phase equilibrium LIQ-(B_xC)-SiB_6 at 1973 K (1700 °C) still needs to be determined. The experimental results from the present work suggest a narrow composition range for the two-phase equilibrium between the liquid phase and a silicon-rich (B_xC) phase at 1973 K (1700 °C). Thus, comparison of Telle's results at 2323 K (2050 °C) and the present work at 1973 K (1700 °C) suggests that an increase in the temperature leads to carbon enrichment of the (B_xC) phase with an almost constant silicon content, resulting to a wider composition range of (B_xC) phase in equilibrium with the liquid phase.

Concerning the other phase equilibria on the B-rich side of the (B_xC) solid solution, an arbitrary composition of Si-containing (B_xC) in equilibrium with SiB_6 and (SiB_n) phases is proposed as no data has been reported in the literature (open circle, **Fig. 7b**). This suggests that the SiB_6 phase might be in equilibrium with (B_xC) with different Si contents. Finally, the silicon solubility in (B_xC) might continue to decrease approaching the (β-B)-(B_xC)-(SiB_n) three-phase equilibrium and then in the (β-B)-(B_xC) two-phase equilibrium.

From a thermodynamic point of view, it is noted that the modelling by Chen *et al*. [16] does not consider the substitution mechanism proposed by Telle [2], i.e. formation of a C-B-(C,Si) linear chain at low Si content and then substitution of Si in the icosahedral B1 and B2 sites

leading to the formation of $B_{11}(C,Si)$. Chen *et al.* used a sublattice model based on structure determination by Werheit *et al.* for the thermodynamic modelling of the (B_xC) phase, such as $(B_{12},B_{11}C)_1(B_2Va,C_2B,B_2C,Si_2)_1$ [38]. The model by Chen *et al*. for the (B_xC) phase includes the possibility of Si substitution, but introduced a Si_2 species instead of the "CBSi" species as proposed by Telle [2]. This suggests that the model of the (B_xC) phase might be modified to better account for the crystallography of the (B_xC) phase and the substitution mechanism proposed by Telle. Also, our experimental results and those of Telle suggest that the model parameters in the thermodynamic modelling by Chen *et al*. of the (B_xC) phase need to be revised to better represent the higher Si content of this phase.

A boron rich phase containing 5.4 at.% Si by EPMA (5.9 ± 0.1 at.% Si by EDS, **Table 2**) at 1973 K (1700 °C) was identified in equilibrium with stoichiometric SiB_6 and was considered to be the (SiB_n) solid solution. Moreover, **Fig. 6** illustrates an Si composition gradient extending from the SiB_6/(SiB_n) phase interface. The experimental (SiB_n) composition found at the interface with SiB_6 concurs with the upper limit of the reported solubility of Si in (SiB_n). Armas *et al*. [32] found the solubility to be 5.4 at.% Si at 1873 K (1600 °C) and 5.7 at.% Si at 2173 K (1900 °C) (filled squares, **Fig. 8**), and the maximum solubility value reported as 6.25 at% Si at 2123 K (1850 °C) is in agreement with 6.13 at% Si at 2137 K (1864 °C) found by Viala *et al.* [27]. In addition, **Fig. 8** shows the solubility limits from literature data [32] for the two-phase equilibrium of (SiB_n) and the (β-B) solid solution (dashed lines). The Si composition of the (SiB_n) phase of the (SiB_n)/(β-B) interface is expected to be less than 2 at.% Si (< 1.6 at.% Si at 1873 K (1600 °C) [32]; < 2 at.% Si at 1973 K (1700 °C) [34]). It is noted that the thermodynamic modelling by Chen *et al.* with a calculated composition at 2.9 at.% Si at 1973 K (1700 °C) (solid lines, **Fig. 8**) overestimates the composition of (SiB_n) in equilibrium with (β-B). Thus, we can conclude that, given the measured composition range from the SiB_6/(SiB_n)

interface and the minimum measured value of 2.2 at.% Si (5.43 wt.% Si, **Fig. 6**) from this experimental study, a Si composition gradient is observed within the (SiB_n) phase on **Fig. 6**.

The experimentally determined phase compositions in the diffusion couple are consistent with the 1973 K (1700 °C) isothermal section (**Fig. 7b**) leading to the following reaction layer sequence of SiC/(B_xC)/SiB_6/(SiB_n)/(β-B), and suggest that silicon and carbon might diffuse towards the center of the diffusion couple, whereas boron might diffuse in the opposite direction. This is partly consistent with the measured composition profiles given in **Fig. 3**: boron compositions in the different phases of the reaction sequence decreased from pure boron to SiC; and carbon compositions followed the same tendency from SiC to boron. However, the silicon composition profile showed a bump through the SiB_6 layer (**Fig. 3**), raising the question about silicon diffusion through the reaction sequence. The driving force behind constituent diffusion of a system is the difference in chemical potential of the constituent within the phases and following Kirkaldy's principles [57], the diffusion process of constituents aligns with a negative chemical potential gradient through the reaction sequence. The chemical potential diagrams for the elements were calculated from the thermodynamic modelling by Chen *et al*. [16] and that of silicon is given in **Fig. 9**. The blue dashed line represents the calculated Si chemical potential along the observed reaction layers from SiC to (β-B), agreeing with the observed two-phase equilibria at the interfaces. Thus, it can be concluded that, even if SiB_6 is an Si-rich phase in the reaction sequence, silicon diffuses from SiC to (β-B) through a negative chemical potential gradient. Concerning carbon (**Fig. 10a**) and boron (**Fig. 10b**), thermodynamic calculations show a decrease in the chemical potential of boron within the phase sequence from (β-B) to SiC, while that of carbon increases (**Fig. 10**). In addition, the reaction layers (blue dashed line in **Fig. 7b**) intersect the initial B-SiC composition line of the diffusion couple respecting the principle of mass conservation [57]. Finally, each interface of the reaction layer sequence maintains a local thermodynamic equilibrium [57]. In conclusion, B, C and Si are constituents

that diffuse following negative chemical potential gradients and the reaction layers sequence observed in the 1973 K (1700 °C) B/SiC diffusion couple represents a diffusion path.

Beyond the spatial phase sequence observed, a temporal sequence is discussed by identifying the initial phase formed. At the early stage of the reaction, the B-SiC interface likely undergoes a local metastable equilibrium that evolves with time and temperature. The B-C-Si isothermal section at 1973 K (1700 °C) (**Fig. 1b**) suggests that SiC could initially be in equilibrium with either C, (B_xC), or a boron-rich liquid phase (up to 27 at.% B). Lee *et al*. [58] propose that, given the B-SiC metastable equilibrium, the phase with the highest driving force for formation under the local interfacial equilibrium would be the first to be formed. Based on the driving force calculations for the B-C-Si system at 1973 K (1700 °C) (**Fig. 11**), (B_xC) exhibits the highest driving force among all stable phases, suggesting it might be the initial phase forming at the B-SiC interface. This finding is further supported by calculations (not shown here) across a temperature range of 1273-1973 K (1000-1700 °C), consistently indicating (B_xC) possesses the highest driving force compared to C or the liquid phase.

(B_xC) formation is explained by the reaction of boron with SiC and should lead to the release of Si, which is liquid at the temperature of the experiment. Therefore, a liquid phase should be formed during the first stage of interaction. However, there is no clear evidence of a liquid phase in the final microstructure the B-SiC diffusion couple after 8 h at 1973 K (1700 °C). This suggests that the liquid phase was formed as a transitional phase which then disappeared during the interaction with time. The only way to obtain evidence of its formation would be to perform new experiments for shorter duration times, an objective that is out of the scope of the present paper, but that could be of interest for a future paper.

Additionally, the formation of (B_xC) as the first phase during B-SiC interaction has been experimentally observed in CVD studies, where a (B_xC) layer forms upon reaction between a

SiC substrate and a boron-rich gas environment [10], corroborating the results from these thermodynamic calculations.

6 Conclusion

This study investigated the reactivity between boron and silicon carbide (SiC) at 1973 K (1700 °C) for 8 h using a diffusion couple technique. Analysis of the reaction zone revealed the formation of intermediate phases through the following reactivity sequence: SiC/(B_xC)/SiB_6/(SiB_n)/(β-B), which is a diffusion path. Notably, we experimentally determined and discussed the solubility limits of (β-B), (SiB_n), SiC, and (B_xC) at 1973 K (1700 °C). The boron carbide (B_xC) layer exhibited a composition gradient (12.4-13.7 at.% C) with an average silicon content of 2.0 at.%. In addition, the experimental study leads to a redefinition of the phase equilibria in the 1973 K (1700 °C) isothermal section of the B-C-Si system.

These findings support the effectiveness of the existing thermodynamic description by Chen *et al*. [16] for predicting overall phase equilibria in the B-Si-C system. It thus provides a sufficient basis for thermodynamic modelling which will serve as the foundation for calculating CVD deposition diagrams and other calculations aimed at understanding the CVD growth of (B_xC) on 4H-SiC.

However, the composition limits of the (B_xC) phase suggest a need for further experiments, particularly regarding Si solubility in (B_xC) and the related phase equilibria in the ternary system. Future work will focus on reassessing the B-C-Si system, with an emphasis on the Si-B binary system (especially the (β-B) and (SiB_n) phases) and Si solubility in (B_xC). This ongoing research will provide deeper insights into the interfacial reactivity between B and SiC.

Acknowledgments

The authors gratefully acknowledge Sandrine Dankic Cottrino (MATEIS, INSA Lyon) for the uniaxial hot pressing of the 1700 °C B/SiC diffusion couple. The authors also thank the CTmu (Centre Technologique des Microstructures, Lyon), especially Xavier Jaurand for their help and advice during SEM-EDS characterizations.

References

1. H. J. Seifert, F. Aldinger, “Phase Equilibria in the Si-B-C-N System”, in High Performance Non-Oxide Ceramics I, ed: M. Jansen, Berlin, Heidelberg, Springer, 2002, p. 1–58
2. R. Telle, “Structure and Properties of Si-Doped Boron Carbide”, in The Physics and Chemistry of Carbides, Nitrides and Borides, ed: R. Freer, Dordrecht, Springer Netherlands, 1990, p. 249–267
3. V. Domnich, S. Reynaud, R. A. Haber, M. Chhowalla, “Boron Carbide: Structure, Properties, and Stability under Stress”, Journal of the American Ceramic Society, 2011, 94(11), p. 3605–3628
4. D. Gosset, “Absorber materials for Generation IV reactors”, in Structural Materials for Generation IV Nuclear Reactors, ed: P. Yvon, Woodhead Publishing, 2017, p. 533–567
5. H. Werheit, “On Microstructure and Electronic Properties of Boron Carbide”, Advances in Ceramic Armor X, 2014, p. 87–102
6. H. Werheit, “On excitons and other gap states in boron carbide”, Journal of Physics: Condensed Matter, 2006, 18(47), p. 10655–10662
7. A. Ahmad, N. J. Ianno, P. G. Snyder, D. Welipitiya, D. Byun, P. A. Dowben, “Optical properties of boron carbide (B_5C) thin films fabricated by plasma-enhanced chemical-vapor deposition”, Journal of Applied Physics, 1996, 79(11), p. 8643–8647
8. K. Rasim, R. Ramlau, A. Leithe-Jasper, T. Mori, U. Burkhardt, H. Borrmann, W. Schnelle, C. Carbogno, M. Scheffler, Y. Grin, “Local Atomic Arrangements and Band Structure of Boron Carbide”, Angewandte Chemie International Edition, 2018, 57(21), p. 6130–6135
9. Y. Benamra, “Dépôt chimique en phase vapeur de BxC sur 4H-SiC : de l’étude thermodynamique à l’hétéroépitaxie” (Chemical vapor deposition of BxC on 4H-SiC: from thermodynamics to heteroepitaxy), Ph.D. Thesis, Université Claude Bernard - Lyon I, 2023, in French
10. Y. Benamra, L. Auvray, J. Andrieux, F. Cauwet, M. Gutierrez, F. Lloret, D. Araujo, R. Bachelet, B. Canut, G. Ferro, “Mechanism of Heteroepitaxial Growth of Boron Carbide on the Si-Face of 4H-SiC”, Crystal Growth & Design, 2025, 25(5), p. 1506–1513
11. R. Kieffer, G. Leimer, P. Ettmayer, E. Gugel, Investigations in the system Boron-Carbon-Silicon, Berichte der Deutschen Keramischen Gesellschaft, 1972, 49(2), p. 41–46
12. P. Dörner, Konstitutionsuntersuchungen an Hochtemperaturkeramiken des Systems B-Al-C-Si-N-O mit Hilfe thermodynamischer Berechnungen, Ph.D. Thesis, Universität Stuttgart, 1980, in German

13. S. Lim, H. Lukas, “Thermodynamische Optimierung des Systems BC-Si und seiner Randsysteme”, DFG, Hochleistungskeramik, Herstellung, Aufbau und Eigenschaften, VCh, Weinheim, 1995, p. 605–616, in German
14. B. Kasper, Phasengleichgewichte im System B-C-N-Si, Ph.D. Thesis, Universität Stuttgart, 1996, in German
15. K. Korniyenko, Materials Science International Team, MSIT®, “B-C-Si Ternary Phase Diagram Evaluation Phase diagrams, crystallographic and thermodynamic data”, Datasheet from MSI Eureka in SpringerMaterials, ed: G. Effenberg, MSI Materials Science International Services GmbH
16. H. M. Chen, H. Y. Qi, F. Zheng, L. B. Liu, Z. P. Jin, “Thermodynamic assessment of the B–C–Si system”, Journal of Alloys and Compounds, 2009, 481(1–2), p. 182–189
17. J. Gröbner, H.L. Lukas, F. Aldinger, “Thermodynamic calculation of the ternary system Al-Si-C”, Calphad, 1996, 20(2), p. 247–254
18. J.-C. Zhao, “Chapter Seven - Phase Diagram Determination Using Diffusion Multiples”, in Methods for Phase Diagram Determination, ed: J.-C. Zhao, Oxford, Elsevier Science Ltd, 2007, p. 246–272
19. F.J.J. van Loo, “Multiphase diffusion in binary and ternary solid-state systems”, Progress in Solid State Chemistry, 1990, 20, p. 47-99
20. A. Kodentsov, A. Paul, “Chapter 6 - Diffusion Couple Technique: A Research Tool in Materials Science”, in Handbook of Solid State Diffusion, Volume 2, eds: A. Paul, S. Divinski, Elsevier, 2017, p. 207–275
21. D. Drouin, A. R. Couture, D. Joly, X. Tastet, V. Aimez, R. Gauvin, “CASINO V2.42—A Fast and Easy-to-use Modeling Tool for Scanning Electron Microscopy and Microanalysis Users”, Scanning, 2007, 29(3), p. 92–101
22. J.-L. Pouchou, F. Pichoir, “Un nouveau modèle de calcul pour la microanalyse quantitative par spectrométrie de rayons X. Partie 1: Application à l’analyse d’échantillons homogènes, La Recherche Aerospatiale”, 1984, p. 167–191, in French
23. J.-O. Andersson, T. Helander, L. Höglund, P. Shi, B. Sundman, “Thermo-Calc & DICTRA, computational tools for materials science”, Calphad, 2002, 26(2), p. 273–312
24. P. T. B. Shaffer, “A review of the structure of silicon carbide”, Acta Crystallographica Section B: Structural Crystallography and Crystal Chemistry, 1969, 25(3), p. 477–488
25. A. Raynaud, « Propriétés physiques et électroniques du carbure de silicium (SiC) », Editions T.I. | Techniques de l’Ingénieur, 2007, in French
26. R. I. Scace, G. A. Slack, “Solubility of Carbon in Silicon and Germanium”, The Journal of Chemical Physics, 1959, 30(6), p. 1551–1555
27. J. C. Viala, R. Hillel, J. Bouix, “Alliages bore-silicium riches en bore partie II: Préparation d’alliages homogènes, analyse, croissance crystalline”, Journal of the Less Common Metals, 1980, 71(2), p. 207–218, in French
28. R. W. Olesinski, G. J. Abbaschian, “The B−Si (Boron-Silicon) system”, Bulletin of Alloy Phase Diagrams, 1984, 5(5), p. 478–484
29. A.I. Zaitsev, “Thermodynamic Properties and Phase Equilibria in the Si-B System”, Russian Journal of General Chemistry, 2002, 72(2), p. 183–192
30. J. Roger, V. Babizhetskyy, J.-F. Halet, R. Guérin, “Boron-silicon solid solution: synthesis and crystal structure of a carbon-doped boron-rich SiB n (n∼30) compound”, Journal of Solid State Chemistry, 2004, 177, p. 4167–4174

31. A. Zhang, L. Wu, Z. Li, “Predicted structural evolution and detailed insight into configuration correlation, mechanical properties of silicon–boron binary compounds”, RSC Advances, 2017, 7(26), p. 16109–16118
32. B. Armas, G. Male, D. Salanoubat, C. Chatillon, M. Allibert, “Determination of the boron-rich side of the B–Si phase diagram”, Journal of the Less Common Metals, 1981, 82, p. 245–254
33. G. Male, D. Salanoubat, “Phase riche en bore dans le système bore-silicium”, Rev. Int. Hautes Temp. Refract, 1981, 18, p. 109–120, in French
34. L. Chen, T. Goto, M. Mukaida, M. Niino, T. Hirai, “Phase Diagram and Thermoelectric Property of Si-B System Ceramics”, Journal of The Japan Society of Powder and Powder Metallurgy, 1994, 41, p. 1299–1303
35. O. Sologub, Y. Michiue, T. Mori, “Boron carbide, B13-xC2-y (x = 0.12, y = 0.01)”, Acta Crystallographica Section E: Structure Reports Online, 2012, 68(8), p. i67–i67
36. H. Werheit, “Boron carbide: Consistency of components, lattice parameters, fine structure and chemical composition makes the complex structure reasonable”, Solid State Sciences, 2016, 60, p. 45–54
37. P. F. Rogl, J. Vřešťál, T. Tanaka, S. Takenouchi, “The B-rich side of the B–C phase diagram”, Calphad, 2014, 44, p. 3–9
38. H. Werheit, U. Kuhlmann, M. Laux, R. Telle, “Solid solutions of silicon in boron-carbide-type crystals”, Journal of Alloys and Compounds, 1994, 209(1), p. 181–187
39. S. Gierlotka, O. Y. Oleksyn, B. F. Palosz, “Si-C-B Systems Synthesized by SHS Method: Phase Diagram and Crystal Structure Evolution”, Materials Science Forum, 1994, 166–169, p. 529–534
40. S. S. Hovden, “A TEM Study of Boron-implanted Cubic Silicon Carbide”, for Solar Cell Applications, Master thesis, NTNU, 2016
41. P. T. B. Shaffer, “Solubility of boron in alpha silicon carbide”, Materials Research Bulletin, 1970, 5(7), p. 519–521
42. Y. Murata, R. Smoak, Y. Somiya, S. Saito, “Densification of Silicon Carbide by the addition of BN, BP and B4C and Correlation to their Solid Solubilities”, Proceedings of the International Symposium on Factors in Densification and Sintering of Oxide and Nonoxide Ceramics, 1978, p. 382–399
43. M. K. Linnarsson, M. S. Janson, N. Nordell, J. Wong-Leung, A. Schöner, “Formation of precipitates in heavily boron doped 4H-SiC”, Applied Surface Science, 2006, 252(15), p. 5316–5320
44. Y. Gao, S. I. Soloviev, T. S. Sudarshan, “Investigation of boron diffusion in 6H-SiC”, Applied Physics Letters, 2003, 83(5), p. 905–907
45. H. H. Woodbury, G. W. Ludwig, “Electron Spin Resonance Studies in SiC”, Physical Review, 1961, 124(4), p. 1083–1089
46. K. L. More, C. H. Carter, J. Bentley, W. H. Wadlin, L. Lavanier, R. F. Davis, “Occurrence and Distribution of Boron-Containing Phases in Sintered β-Silicon Carbide”, Journal of the American Ceramic Society, 1986, 69(9), p. 695–698
47. H. Batha, I. Hardy, “Resistance anomaly in p-type silicon carbide”, in Proceedings of an International Conference on Silicon Carbide, Florida, 1974, p. 435–442
48. Y. Tajima, W. D. Kingery, “Solid Solubility of Aluminum and Boron in Silicon Carbide”, Journal of the American Ceramic Society, 1982, 65(2), p. 27–29

49. S. G. Sridhara, L. L. Clemen, R. P. Devaty, W. J. Choyke, D. J. Larkin, H. S. Kong, T. Troffer, G. Pensl, “Photoluminescence and transport studies of boron in 4H SiC”, Journal of Applied Physics, 1998, 83(12), p. 7909–7919
50. T. Troffer, M. Schadt, T. Frank, H. Itoh, G. Pensl, J. Heindl, H. P. Strunk, M. Maier, “Doping of SiC by Implantation of Boron and Aluminum”, physica status solidi (a), 1997, 162(1), p. 277–298
51. C.-H. Pai, “Thermoelectric Properties of Boron Compound-Doped α-SiC Ceramics”, Journal of the Ceramic Society of Japan, 2004, 112(1302), p. 88–94
52. P. Carvalho, A. Thørgesen, Q. Ma, D. Nielsen Wright, S. Diplas, A. Galeckas, A. Azarov, V. Jokubavicius, J. Sun, M. Syväjärvi, B. G. Svensson, O. M. Løvvik, “Boron-doping of cubic SiC for intermediate band solar cells: a scanning transmission electron microscopy study”, SciPost Physics, 2018, 5(3), p. 021
53. M. K. Kolel-Veetil, R. M. Gamache, N. Bernstein, R. Goswami, S. B. Qadri, K. P. Fears, J. B. Miller, E. R. Glaser, T. M. Keller, “Substitution of silicon within the rhombohedral boron carbide (B4C) crystal lattice through high-energy ball-milling”, Journal of Materials Chemistry C, 2015, 3(44), p. 11705–11716
54. M. Xinmin, N. Cewen, C. Kefeng, “Structural Characteristics and Quantum Chemistry Calculation of Si-Doped Boron Carbides”, MRS Online Proceedings Library, 1998, 538(1), p. 579–584
55. Z. Li, R. C. Bradt, “Thermal expansion and thermal expansion anisotropy of SiC polytype”, Journal of Applied Physics, 1986, 60(2), p. 612–614
56. T. R. Pilladi, G. Panneerselvam, S. Anthonysamy, V. Ganesan, “Thermal expansion of nanocrystalline boron carbide”, Ceramics International, 2012, 38(5), p. 3723–3728
57. J. S. Kirkaldy, L. C. Brown, “Diffusion Behaviour in Ternary, Multiphase Systems”, Canadian Metallurgical Quarterly, 1963, 2(1), p. 89–115
58. B.-J. Lee, “Prediction of interfacial reactions using thermodynamic calculation and diffusion simulation”, CALPHAD and Alloy Thermodynamics, eds. P. E. A. Turchi, A. Gonis, R. D. Shull, TMS, Warrendale, PA, 2002, p. 131–144

Figure Captions

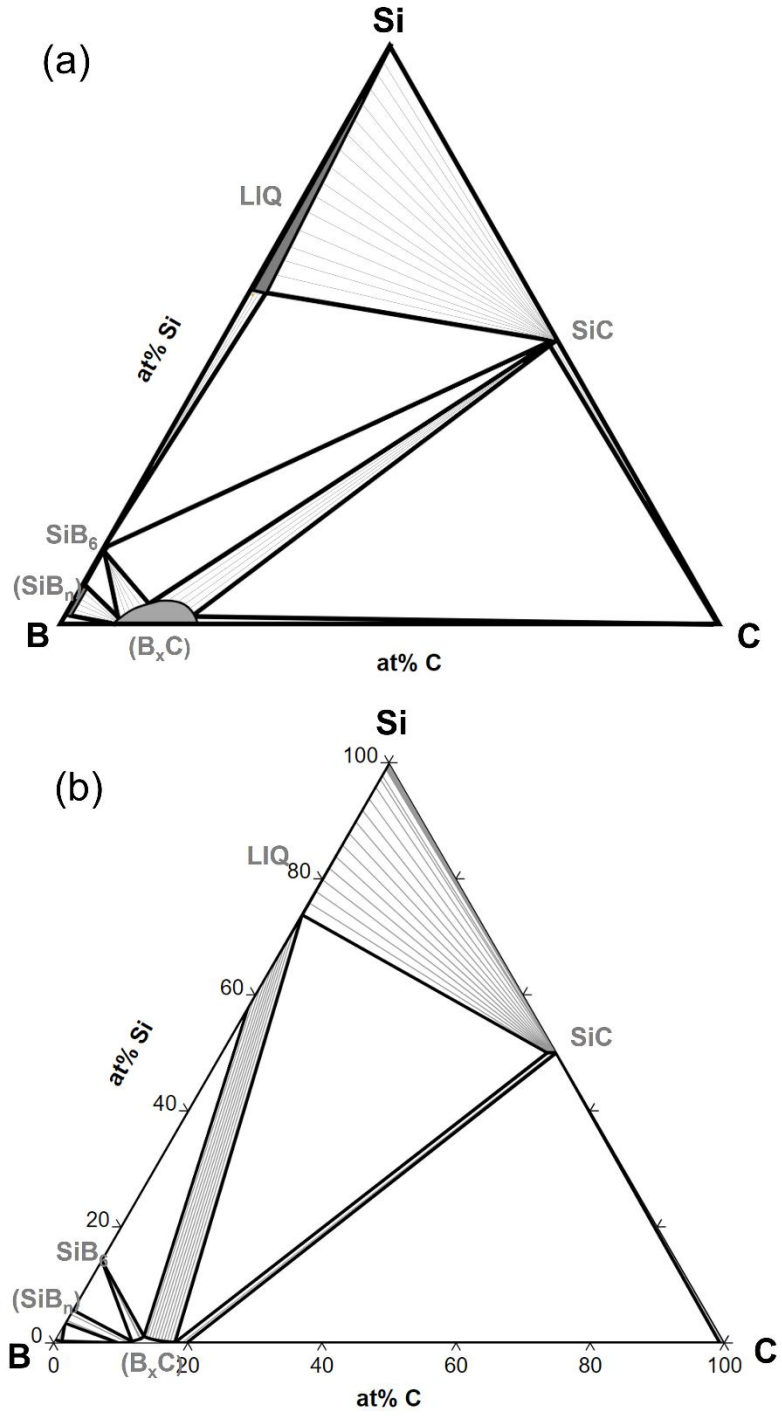

Fig. 1 Isothermal section of B-C-Si system at 1973 K (1700 °C): **(a)** re-schematized figure as proposed by Kieffer *et al*. [11] and **(b)** as calculated from the thermodynamic modelling by Chen *et al*. [16]

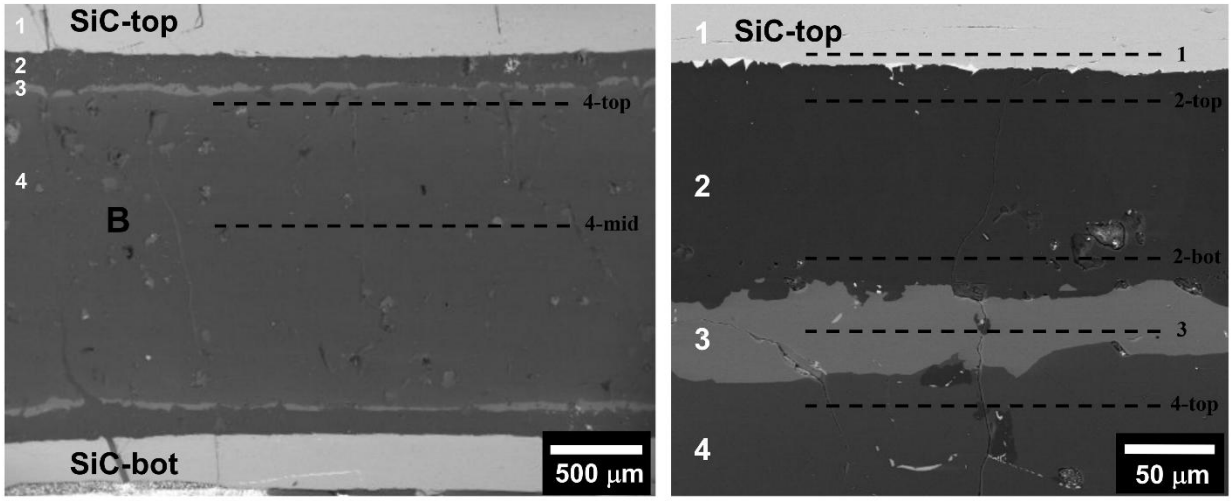

Fig. 2 Backscattered electron (BSE) images of a cross-sectional cut of the 1973 K (1700 °C)-8 h diffusion couple: overview (a) and higher magnification image (b) of the upper zone of the B/SiC diffusion couple. The dashed lines represent the location of the different EDS-EPMA line scans

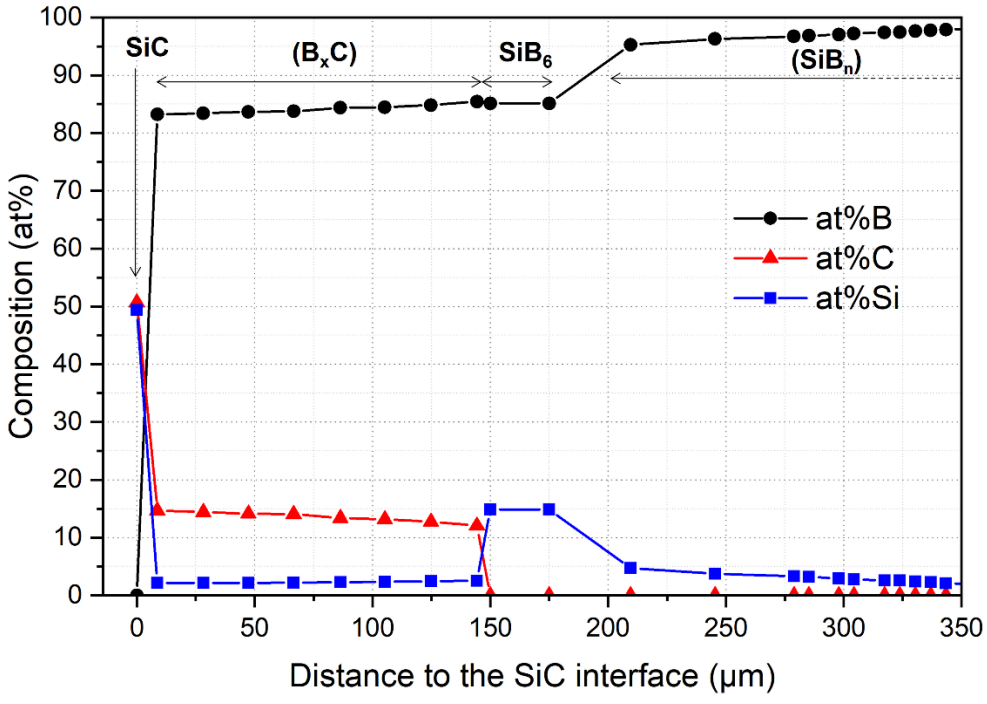

Fig. 3 Composition profiles of boron, carbon, and silicon measured through the interfacial reaction sequence of the 1973 K (1700 °C)-8h diffusion couple using EDS

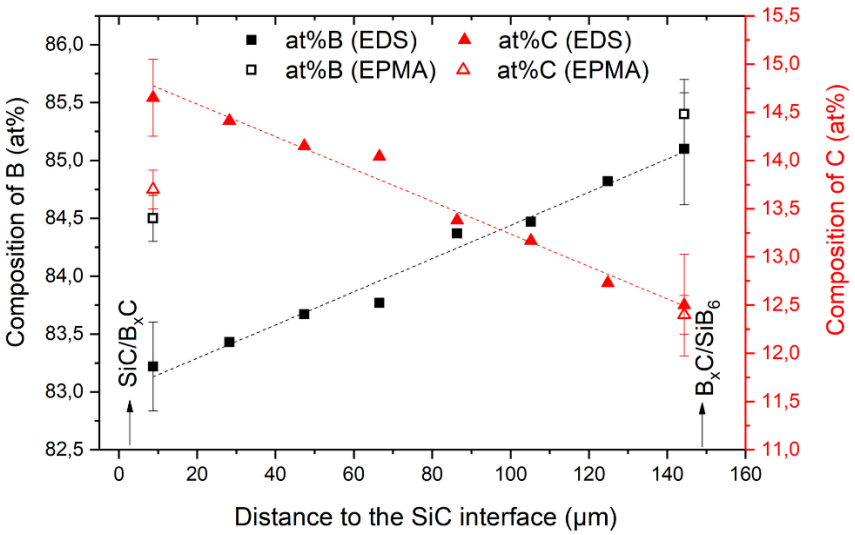

Fig. 4 Evolution of the boron (square) and carbon (triangle) content through the (B_xC) layer extending from the SiC interface after 8 h thermal treatment at 1973 K (1700 °C). EDS (filled symbols) and EPMA (open symbols) results. Dotted lines represent the trend for B and C contents through the layer from EDS measurements

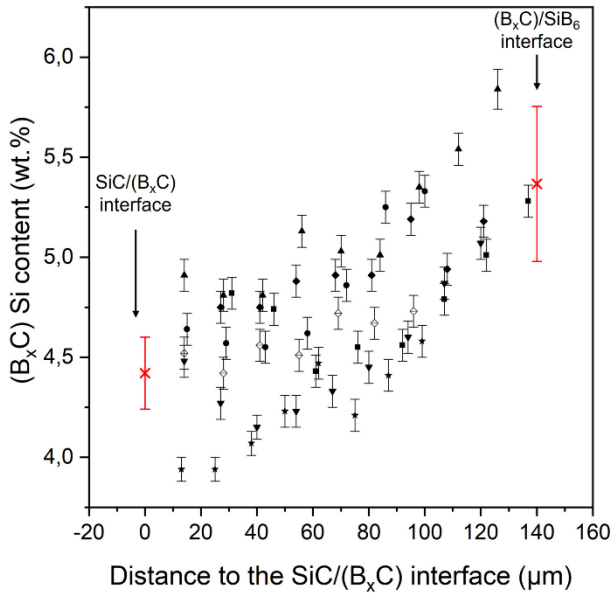

Fig. 5 Evolution of silicon content through the (B_xC) layer extending from the SiC/(B_xC) interface, measured by seven EPMA line scans after 8 h of thermal treatment at 1973 K (1700 °C). Black error bars represent the 95% confidence interval for each measurement. Crosses indicate the average Si content at the interfaces with error bars corresponding to the standard deviations of the measurements

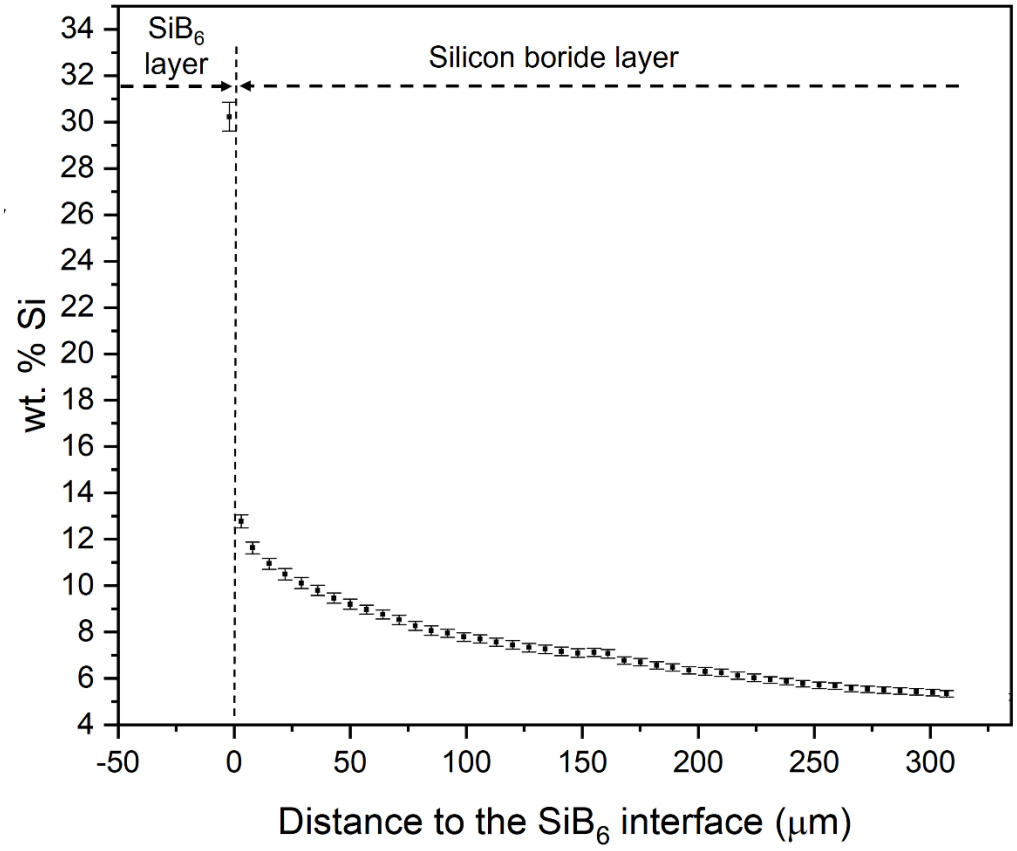

Fig. 6 Evolution of silicon content within the silicon boride layer, starting from the SiB_6/(B_xC) interface toward the center of the diffusion couple, measured with EPMA-WDS measurements after 8 h of thermal treatment at 1973 K (1700 °C). Error bars indicate the standard deviations of the measurements

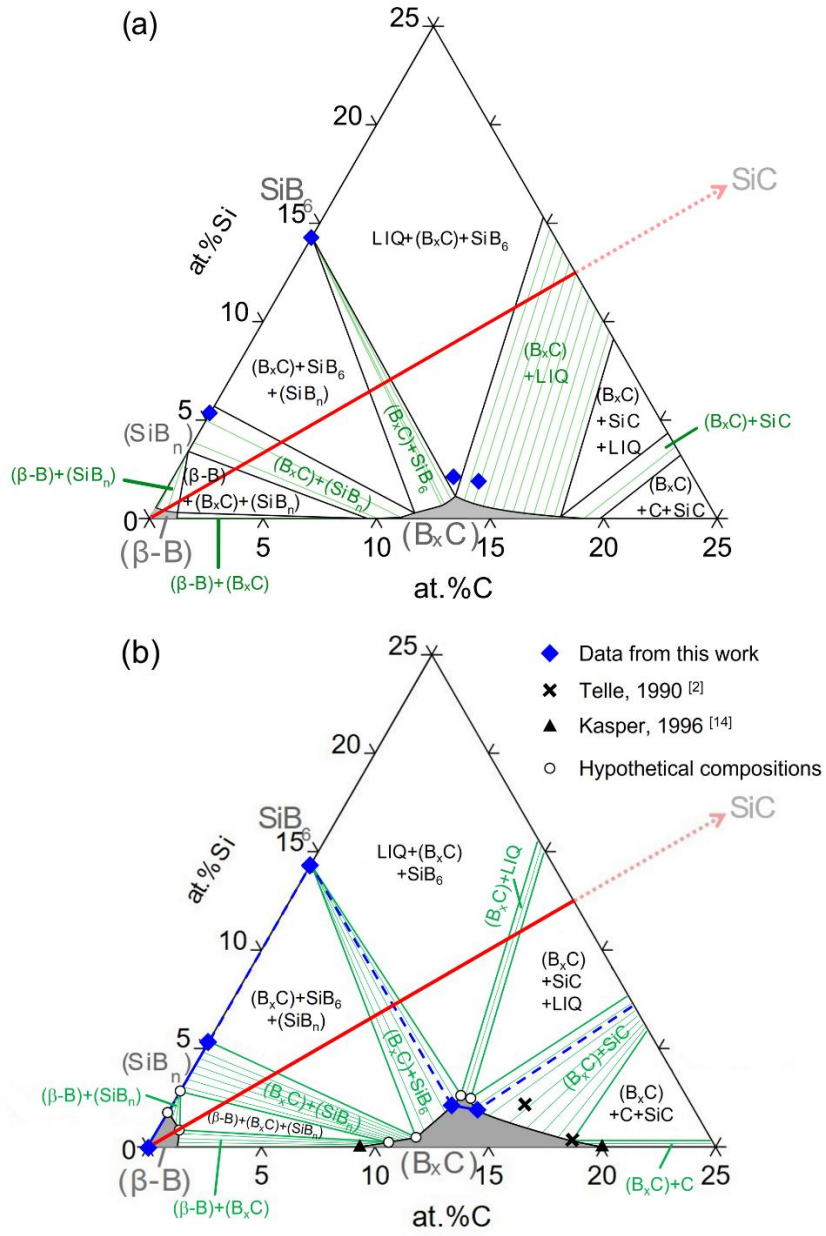

Fig. 7 (a) Isothermal section of the B-C-Si system at 1973 K (1700 °C) calculated using the thermodynamic modelling by Chen *et al*. [16]. The red solid line represents the B-SiC diffusion couple line composition. Experimental EPMA phase compositions are shown as blue-filled diamonds. Green lines represent two-phase equilibria, and grey-colored domains represent the solubility limits of solid solutions. (b) Proposed phase equilibria based on experimental measurements in this work. The blue dashed line indicates the proposed experimental reaction layers sequence. Black-filled triangles and crosses represent experimental data from the literature [2, 14]. Open circles are hypothetical compositions

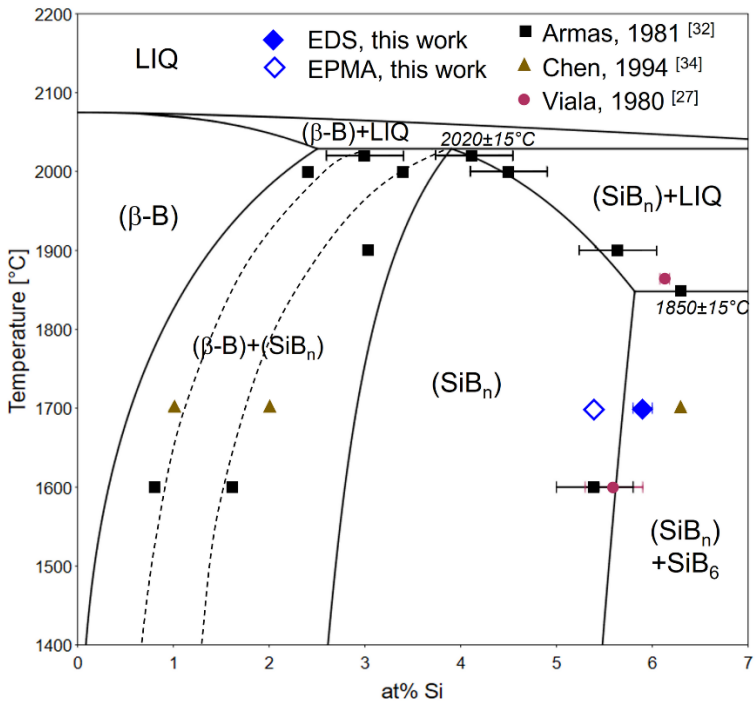

Fig. 8 Calculated binary B-Si phase diagram according to Chen *et al.* [16] (solid lines). The upper (SiB_n) solubility determined in this study is indicated by the blue diamonds. Experimental literature data are from [27, 32, 34]. The dashed lines represent the estimated experimental solubility limits of the (β-B)+(SiB_n) two-phase domain based on literature data

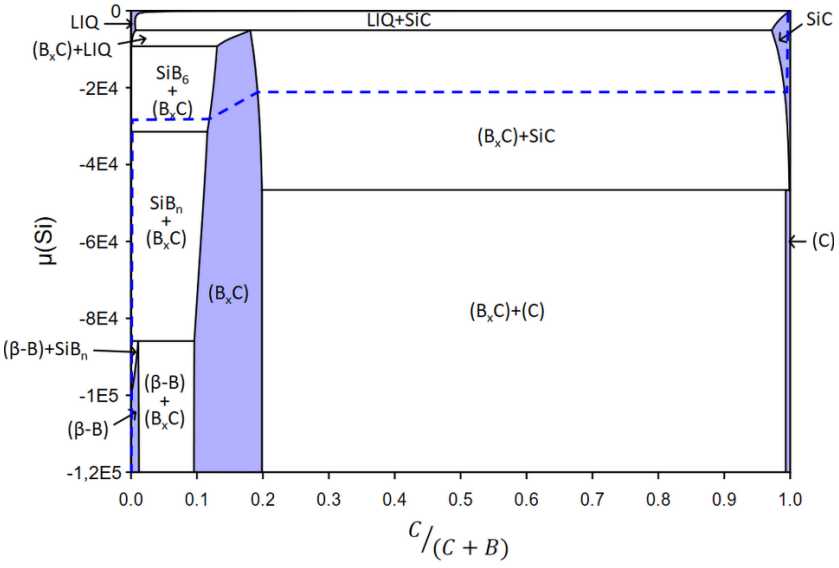

Fig. 9 Silicon chemical potential diagram at 1973 K (1700 °C), based on the thermodynamic modelling by Chen *et al.* [16]. The blue dashed lines represent evolution in the Si chemical potential along the observed reaction layers sequence

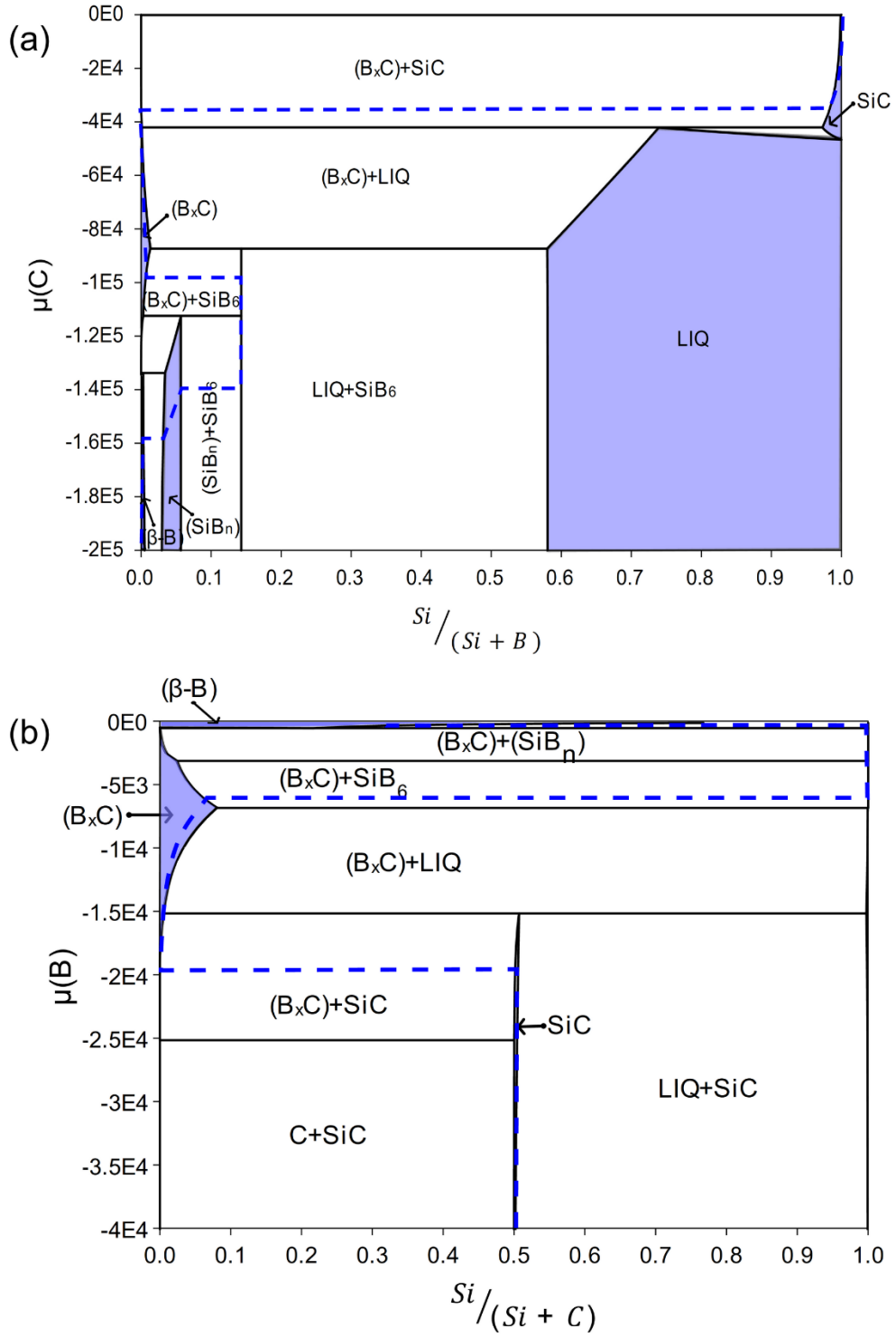

Fig. 10 Carbon (a) and boron (b) chemical potential diagrams at 1973 K (1700 °C), based on the thermodynamic modelling by Chen *et al.* [16]. The blue dashed lines represent evolution in the C (a) and B (b) chemical potentials along the observed reaction layers sequence

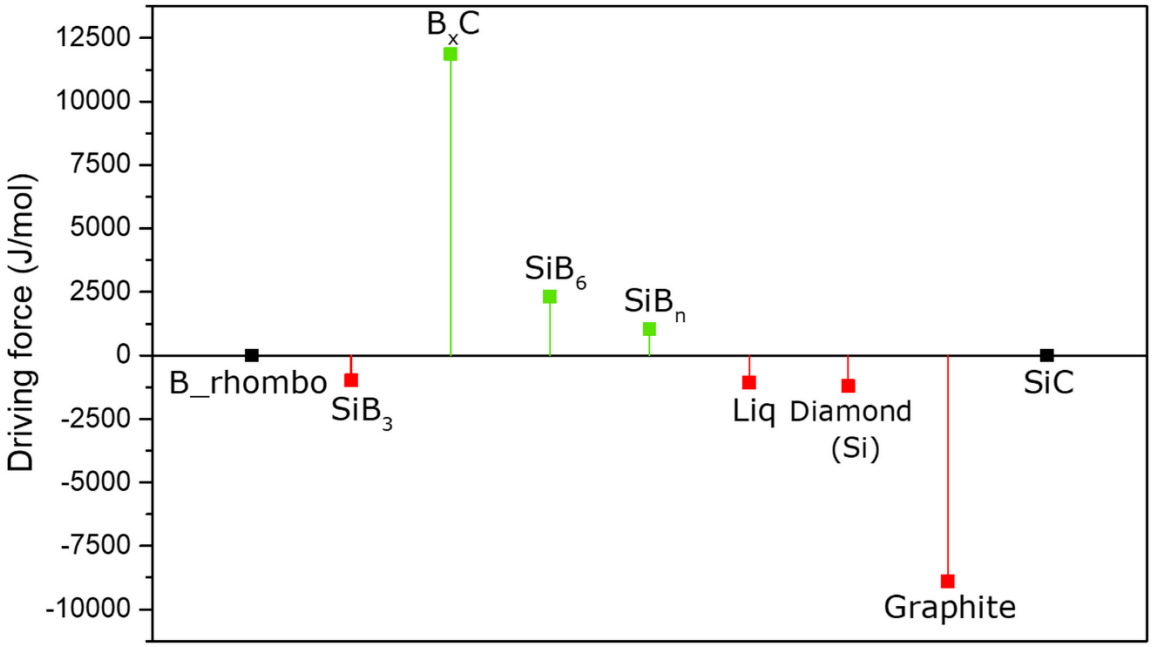

Fig. 11 Driving force calculation for the formation of the different phases of the B-C-Si ternary system when B and SiC react at 1973 K (1700 °C), based on the thermodynamic modelling by Chen *et al*. [16]

Tables

Table 1 Experimental literature data on the solubility of B in SiC

	Temperature	Boron content in SiC	Reference
β-SiC	Unknown (SHS specimen)	3 at.% (1 wt.%)	[39]
	1673 K (1400 °C)	3 at.%	[40]
α-SiC	2723-2773 K (2450-2500 °C)	0.36 at.% (<0.2 wt.%)	[41]
	2473 K (2200 °C)	0.7 at.% (0.4 wt.%)	[42]
	1973 K (1700 °C)	<0.02 at.%	[43]
	2273-2473 K (2000-2200 °C)	<0.1 at.%	[44]

Table 2 EDS and EPMA-WDS measurements of the layers identified in **Fig. 2**

Layer *	Experimental atomic composition			Total weight percent before normalization, wt.%	Phase identified	Quantification technique	Number of independent measurements
	B at.%	C at.%	Si at.%				
1	-	50.3 ± 1.0	49.7 ± 1.0	100.6 ± 0.8	SiC	EDS	9
2 (top)	83.2 ± 0.4	14.7 ± 0.4	2.1 ± 0.1	103.1 ± 0.6	(B_xC)	EDS	10
2 (top)	84.5 ± 0.2	13.7 ± 0.2	1.8 ± 0.1	100.0 ± 0.2	(B_xC)	EPMA-WDS	5
2 (bottom)	85.1 ± 0.5	12.5 ± 0.5	2.4 ± 0.1	100.9 ± 0.5	(B_xC)	EDS	9
2 (bottom)	85.4 ± 0.3	12.4 ± 0.2	2.2 ± 0.2	99.4 ± 0.1	(B_xC)	EPMA-WDS	6
3	85.1 ± 0.2	-	14.9 ± 0.2	99.3 ± 0.8	SiB_6	EDS	10
3	85.68	-	14.32	(101.5)**	SiB_6	EPMA-WDS	1
4 (top)	94.1 ± 0.1	-	5.9 ± 0.1	100.2 ± 0.5	(SiB_n)	EDS	9
4 (top)	94.6	-	5.4	(100.2)**	(SiB_n)	EPMA-WDS	1
4 (middle)	99.5 ± 0.2	-	0.5 ± 0.2	99.6 ± 0.3	(β-B)	EDS	2

** Labelling refers to the different layers in **Fig. 2**. ** Total weight values in parentheses are given for information purposes only and are based on a single measurement.*